J Mater Sci (2007) 42:3607–3612
DOI 10.1007/s10853-006-0240-3

Characterization and wear resistance of laser surface cladding AZ91D alloy with Al + Al_2O_3

Yao Jun · G. P. Sun · C. Liu · S. Q. Jia · S. J. Fang · S. S. Jia

Received: 16 July 2005 / Accepted: 14 April 2006 / Published online: 30 January 2007

Abstract The laser surface cladding of AZ91D magnesium alloy with Al + Al_2O_3 powders was investigated. X-ray diffraction (XRD) was used to identify the phases in the laser cladding layer, and the growth morphology of the boundary zone between the laser surface cladding layer and AZ91D substrate was observed by optical microscope and scanning electron microscope (SEM). The elements mapping scanning analysis on the boundary zone were carried out with energy-dispersive spectrum (EDS). The results showed that the distribution of the Al_2O_3 particles was homogeneous in the laser surface cladding layer; the growth morphology of the boundary zone was found to be in a unique parallel-branching feature. The temperature gradient, the liquidus temperature, the rate of dendrite growth and the rate of pool solidification on the growing fronts affected its formation. Furthermore, compared with the AZ91D substrate, the wear resistance of the laser cladding coatings was improved.

Y. Jun · G. P. Sun · C. Liu · S. Q. Jia · S. J. Fang · S. S. Jia (✉)
Key Laboratory of Automobile Materials of Ministry of Education and Department of Materials Science and Engineering, Jilin University, No. 142 Renmin Street, Changchun 130025, P.R. China
e-mail: sungp@jlu.edu.cn

Y. Jun
Department of Materials Science and Engineering, Inner Mongolia Polytechnic University, No. 226 Aimin Road, Huhhot 010062, P.R. China

Introduction

The continuous and increasing demand for lightweight materials in aerospace and automotive applications encourages the researchers to focus attention on the development of magnesium and its alloys because of their high specific strength and low densities (from 1.74 to 1.85 g cm^{-3}), which is approximately 35% smaller compared to Al-based alloys and 65% smaller than that of Ti-based alloys [1–6]. However, magnesium has a number of undesirable properties including poor corrosion and wear resistance, poor creep resistance and high chemical reactivity, which limit its extensive use in many applications. Recently, Dutta et al. [7] have studied magnesium alloys surface melting with aim to enhance the anti-corrosion and wear resistances, and they concluded that the corrosion and wear resistance were improved. In other efforts, Galun et al. [8] studied laser surface alloying of pure Mg with Al and Al·Ni and found a significant enhancement in wear resistance. The maximum improvement in wear resistances was achieved in laser surface alloying Mg with Al Ni. Although some studies have been carried out to utilize TiC as reinforcement in iron aluminide composites [9–11], few attempts have been so far made on the AZ91D substrate by the laser surface cladding layer as a coating material with Al + Al_2O_3. Moreover, it is well known that the growth morphologies of reinforcement affect strongly the mechanical and physical properties of magnesium and its alloys. On the other hand, it should be mentioned that Al_2O_3, as hard ceramic particles, has a series of excellent properties, e.g. high hardness, stability and low density, and is often used as reinforcing phase in

aluminum alloys. Therefore, Al + Al_2O_3 composites fabricated by laser cladding layer are expected to be a candidate of the wear resistant and anti-corrosion material, and it is necessary to study the morphology and formation of boundary microstructure in the laser cladding AZ91D with Al + Al_2O_3.

In the present work, the aluminum and its oxide composite coatings were fabricated on the AZ91D substrate by laser cladding; a detailed characterization of the laser processed zone and the boundary zone between the laser surface cladding layer and AZ91D substrate has been comprehensively investigated in terms of microstructure, elements and phases. Finally, the wear resistance has also been investigated.

Experimental details

Magnesium alloy substrates that were directly cut from die cast plates of AZ91D components with size of $100 \times 50 \times 3.5$ mm^3 were used as target for laser cladding [12, 13]. These plates were polished with 600-grit SiC paper prior to laser surface treatments in order to produce an unvarying and smooth surface finish, free from mold contaminants and washed with alcohol and dried in air, they were then heated and shortly prepared before the surface cladding was carried out with a Nd: YAG laser (Model HASS 3006D). The powder feeder was a MFP-I type (Metco. Co.) and the powder feed rate was 10–30 g m^{-1}. The laser beam was transmitted by means of optical fiber with an inside diameter of 600 μm, resulting in the homogeneous distribution of intensity. The laser power ranges from 500 to 3000 W, the velocity of work platform ranges from 3 to 28 mm s^{-1}, and the shielding gas was argon with a flow rate of 0.176 1 s^{-1}. The focal length was 142 mm, and the distance of defocusing was 89 mm. A ø3 mm laser spot was used to coupling with shielding gas nozzle diameter. Finally, the wear of the surface cladding specimen was compared with the AZ91D substrate by a wear testing machine (MM-200) with a 3-kg applied load and 300-rpm wheel speed, and Fig. 1 is a schematic illustration of the block-on-wheel sliding wear apparatus.

Microstructure and phase analyses were investigated by using scanning electron microscopy (SEM) (Model JSM-5600, Japan) (SEM) (Model QUANTA 400, Philip) equipped with energy dispersive spectroscopy (EDS) (Model Link-Isis, Oxford) and X-ray diffraction (XRD) (Model D/Max 2500PC Rigaku, Japan).

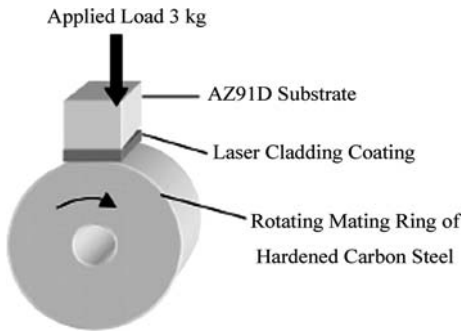

Fig. 1 A schematic illustration of the block-on-wheel sliding wear apparatus

Results

Characterization and morphology of the boundary in the laser cladding coating

XRD result analysis shows that the laser cladding coating (a) has a microstructure consisting of Al and Al_2O_3, and the AZ91D substrate (b) consisting of Mg and $Mg_{17}Al_{12}$, as shown in Fig. 2, which indicates a rapidly solidified Al_2O_3-reinforced composite layer is fabricated using laser surface cladding. Figure 3a shows the cross-section of AZ91D die cast plate specimen after laser cladding. This aspect is a type of AZ91D alloy laser cladding layer, which consists of three zones from the top to the bottom: cladding layer, bond or boundary zone, and substrate. It is evident that the grain size is fine and homogeneous distributed in the surface of cladding layer, as shown in Fig. 3b, which paralleled the plane of the specimen.

The growth morphology of the boundary zone in the laser cladding coating was found to be a unique parallel-branching dendrite, in which the growth fronts

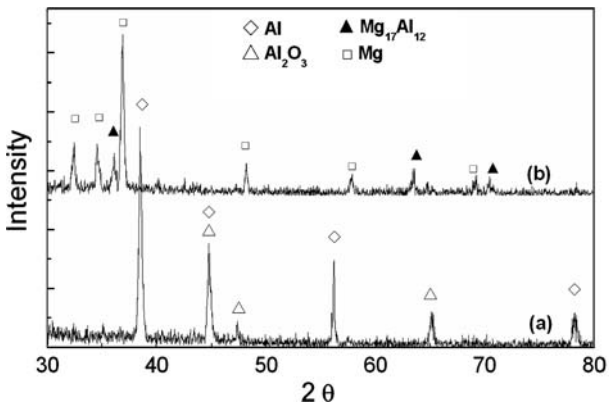

Fig. 2 X-ray diffraction profiles of the top laser cladding surface and the AZ91D substrate

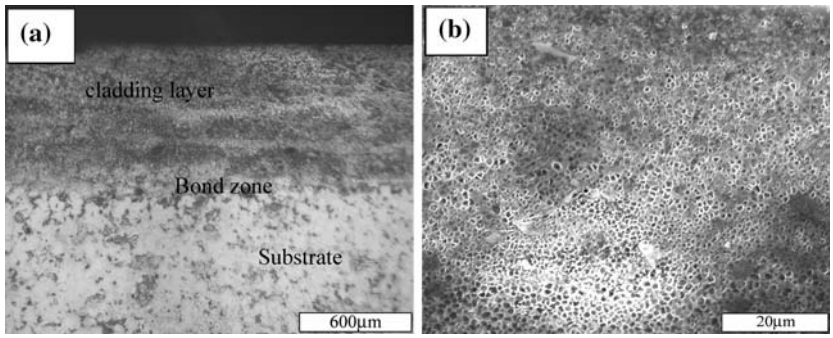

Fig. 3 Micrograph of the (**a**) cross-section showing cladding layer and (**b**) surface of laser cladding with Al + Al_2O_3 (SEM)

have strong radial-dendrites feature, as shown in Fig. 4a and b, it has an epitaxial characteristic from the substrate to the cladding layer and its growth orientation is vertical to the bond line. However, its length is different because of the variation of the scanning speed. When the power is given, the lower scanning speed (Fig. 4b) will cause the dendrites at the bottom of cladding layer to growth longer, however, the higher scanning speed (Fig. 4a) will lead the dendrites to growth shorter. This result from the increasing of scanning speed will reduce the laser–matter interaction time and the laser energy absorbed, leading to the dendrites have little time to grow the longer. However, it is should be also noted that application of too low a scanning speed may lead to surface evaporation and the over melt of substrate, moreover, the application of a high scan speed may cause inadequate melting and intermixing, will lead to a bad wettability and the inhomogeneous distribution of Al and Al_2O_3 particles. Therefore, the choice of a suitable scanning speed under the given power is crucial to achieve uniform intermixing of the alloying elements and hard particles in the surface cladding layer. In the present study conditions, suitable parameters are laser power of 2.0–2.5 kW, scanning speed of 4–8 mm s^{-1} and powder feed rate of 10–15 mg s^{-1}. It should be mentioned that the grain size is fine at the bottom of cladding layer and the size of particles at the top is coarse, as shown in Fig. 4a, which implicated that parts of the particles of Al and Al_2O_3 have been melted in the processing of laser cladding.

Line and mapping scan of elements

To study the distribution of elements in laser cladding coating, the scan of bond zone elements and mapping scanning analysis were carried out (Fig. 5). Micrograph bond zone of the laser surface cladding AZ91D with scanning speed of 6 mm s^{-1}, laser power of 2.5 kW, powder feed of 8 mg s^{-1} and its line scan of Mg, Al, Si and Zn, respectively. It can be seen from line scans of Mg, Al, Si and Zn elements that the white region contains more Al element on the upper of cladding layer, and the dark region contains more Mg element at the bottom of substrate, but the element O did not detected, as shown in Fig. 5. It should be noted that the slow changes of the line scans of magnesium and aluminium in the boundary region suggested the presence of the metallic compound formed by magnesium and aluminium. Figure 6 exhibits the mapping scans of the O, Mg, Al and Zn elements as well as its energy dispersive spectroscopy (EDS). It is evident from Fig. 6a that the distribution of particles at the top of laser cladding layer is uniform and consists of Al, Mg, O, and Zn elements. Moreover, the distribution of element Al in the upper, as shown in Fig. 6e, is more

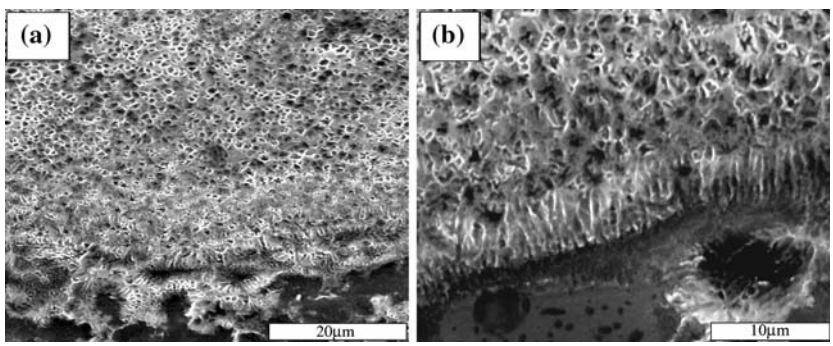

Fig. 4 Micrograph boundary zone of laser cladding AZ91D with a laser scanning speed of (**a**) 10 mm/s and (**b**) 5 mm/s, both laser power is 2.5 kW

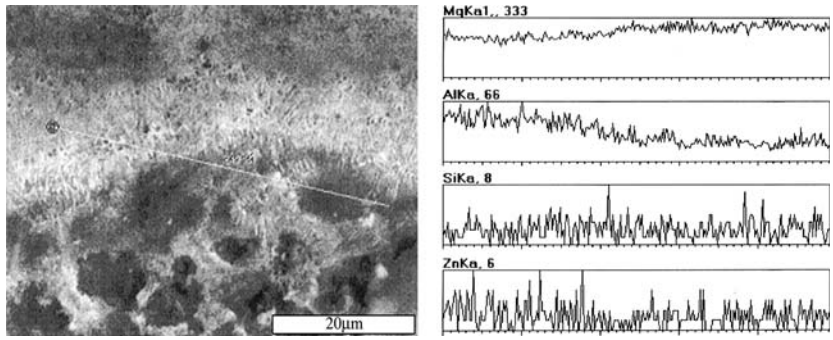

Fig. 5 Micrograph bond zone of the laser surface cladding AZ91D with scanning speed of 6 mm/s, laser power 2.5 kW, powder feed 8 mg/s and its line scan of Mg, Al, Si and Zn, respectively

than that in the bottom, however, that of Mg is reverse in Fig. 6d, and that of O and Zn has a few changes in Fig. 6c and f.

Evaluation of wear resistance of laser surface cladding

Figure 7 shows the wear resistance of the AZ91D substrate (b) and the laser surface cladding layer (a) with $Al + Al_2O_3$. The volume wear of the AZ91D substrate and the laser composite surface were measured by a wear testing machine against hardened steel disc with a 3-kg applied load and 300-rpm wheel speed for a period between 1 min and 1.6 h, and subsequently measuring the wear loss of materials at a regular interval. Figure 7 compares the volume wear of the AZ91D substrate (b) and the same specimen (a) by laser surface cladding (with a power of 2.5 kW, scan

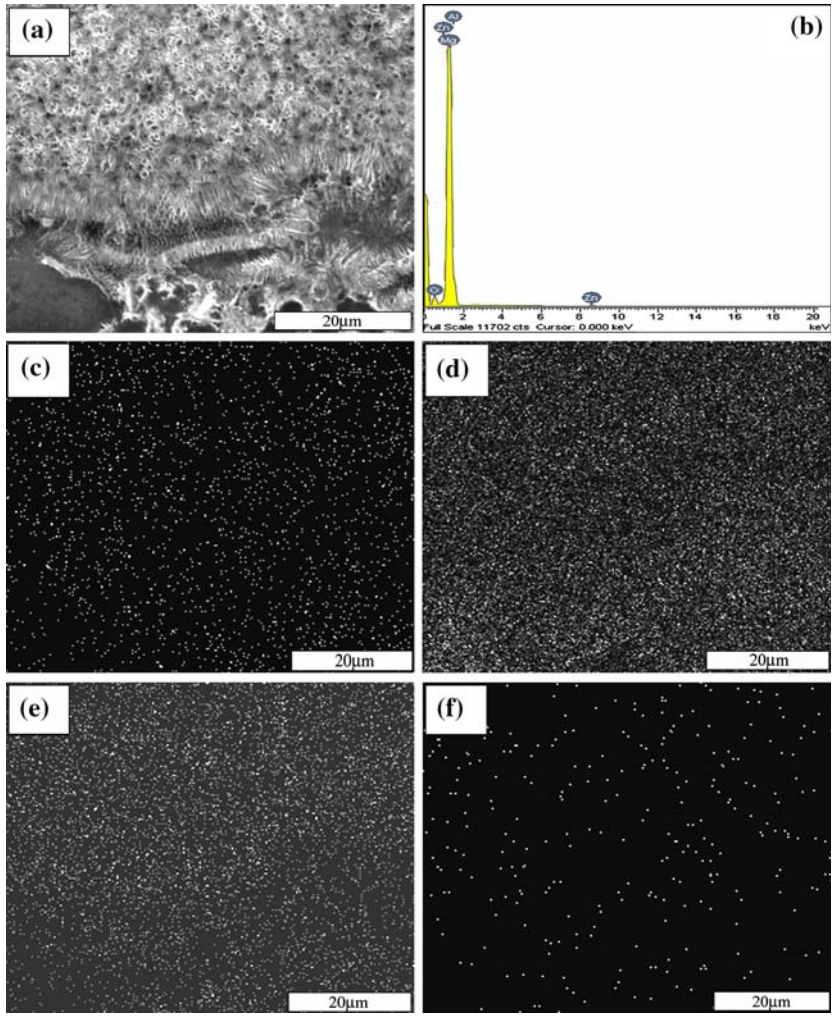

Fig. 6 Micrograph bond zone of the laser surface cladding AZ91D with scanning speed 8 mm/s, laser power 2.5 kW, powder feed 12 mg/s (**a**) and its energy dispersive spectroscopy (**b**) EDS and mapping scans of (**c**) O, (**d**) Mg, (**e**) Al and (**f**) Zn, respectively

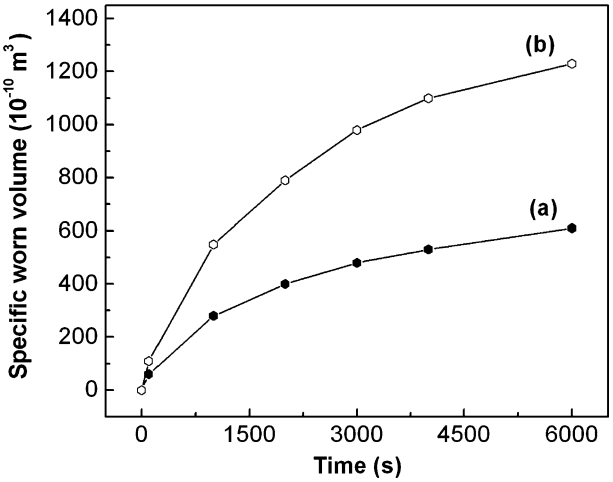

Fig. 7 The comparison of the specific worn volume of the AZ91D substrate (**b**) and the laser cladding coating with Al + Al2O3 (**a**) (with laser power of 2.5 kW and scanning speed of 5 mm s^{-1})

speed of 5 mm s^{-1}) as a function of time. It may be noted that the volume wear is considerably reduced due to laser surface cladding. Volume wear loss of the AZ91D is about 1300×10^{-10} m^3, compared with that of laser surface cladding is 600×10^{-10} m^3 after the 1.6 h of exposure. The superior wear resistance behavior of laser surface cladding layer is attributed to improved microstructure in the surface layer because of the presence of hard ceramic particles Al_2O_3 and aluminium (Figs. 3–6).

Discussion

Formation of parallel-branching dendrite

When the laser pool solidified under high cooling rate, a deviation from the equilibrium diagram during solidification had occurred. Therefore, the formation of parallel-branching dendrite is a consequence of their local growth conditions and nucleation environments. According to the solidification theory, the rate of dendrite growth on the growing fronts υ is correlated to the temperature gradient G_L, the diffusion coefficient of the solute in the laser melt pool D_L, in a high growth rate, and the rate of dendrites υ should follow the inequation [14]

$$\frac{G_L D_L}{\Delta T_0} \leq \upsilon \leq \frac{D_L \Delta T_0}{k\Gamma} \tag{1}$$

where Γ is the coefficient of Gibbs–Thomson and k represents the distribution coefficient of solute. When the variation of υ is in the range of Eq. 1, the parallel-branching dendrite is formed, where $(G_L \Delta T_0/k\Gamma)$ represents the upper limit of the plane growth of absolute stability and $(G_L D_L/\Delta T_0)$ represents a lower limit of the parallel-branching dendrite growth.

$$\Delta T_0 = -mC_0(1 - k_0)/k_0 \tag{2}$$

where m is the slop of liquid in the phase diagram and C_0 is the initial alloy composition, ΔT_0 is a constant represented the spacing of solidification in the phase diagram and independent of the processing parameters. The interface temperature, T, of a faceted/non-faceted eutectic obeys a law of the form [15], for the platelets

$$T = T_1 - \frac{mC_0}{1 + (k-1)\pi^{1/2} e^P Erfc(P^{1/2})} + mC_0 - \frac{\Gamma}{r} \tag{3}$$

and for the dendrites needles

$$T = T_1 - \frac{mC_0}{1 + (k-1)Pe^P \mathrm{Exp}(P)} + mC_0 - \frac{2\Gamma}{r} \tag{4}$$

where T_1 is the liquidus temperature (stable or metastable), k_0 is the equilibrium distribution coefficient of solute, C_0 is the initial alloy composition, P is the Peclet number $(=\upsilon r/2D)$, r is the tip radius of dendrite, *Erfc* is the complementary error function and Exp is the exponential integral function. The maximum tip undercooling temperatures ΔT can be expressed,

$$\Delta T = K\upsilon^{\alpha} \tag{5}$$

where K and α are positive constants with $\alpha = 0.25$–0.5 depending on the actual growth mechanism, under the rapid solidification and laser parameters the undercooling of Mg–Al dendrite needle can be approximated by the Eq. 5 [15, 16]. At the bottom of the melt pool, the value of G_L is higher and υ is lower than that at the top of the melt pool, which made it easy to form the parallel-branching dendrite, as shown in Fig. 2b. In the case of laser cladding AZ91D, υ represents the speed of the eutectic growth front of AZ91D substrate, which was not the growth rate of the Al_2O_3 because most of Al_2O_3 particles did not melt (melt point 2050 °C and laser melt pool was 1500–1700 °C), this is different from the situation of laser remelting.

Effect of convection on the elements distribution

In addition to the temperature gradient, the ultimate rate of dendrite growth, and the undercooling of the melt pool, the convection of the melt pool also affected its microstructure formation. Figure 8 shows

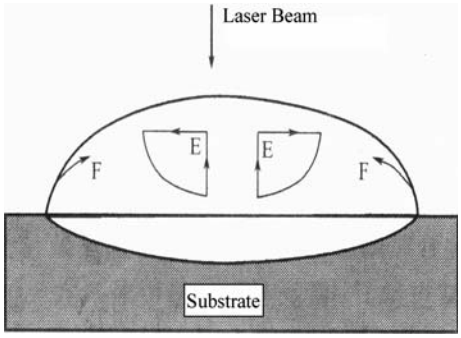

Fig. 8 Model of the convection in laser cladding melt pool

the convection model in the melt pool, in which two sorts of convections exist, i.e. the convection symmetry circle E cycled from the bottom to the central top surface and the convection symmetry F cycled from two sides to the center in the melt pool. In a speckle plane of laser, the energy of center is higher than that of circumference. Therefore, the top temperature on the surface is higher than that of circumference, and convection F, which was not the main convection and only took place on the surface of melt pool, was formed by the surface tension. But in the internal melt pool, the central temperature is also higher than that of the two sides; therefore, convection E was formed. The minority convection F on the surface will bring to the dilution degree increasing and the mixing of substrate and cladding alloys, therefore, it undermined the wettability and the composition the cladding layer. On the other hand, the internal convection E will churn up the melt pool and be beneficial to the homogenous distribution of all alloy elements in the melt pool, but the violent convection E in short time will produce the samdwich microstructure and harmful to the mechanical properties of the cladding layer. Therefore, a proper increasing convection E will be beneficial to the homogeneous microstructure of cladding layer coating, and the convection mainly depended on the laser parameters.

Conclusions

In the present work, the laser cladding composite coatings were fabricated with aluminium and alumina. Wear resistance was evaluated under dry sliding wear conditions as a function of time. The following results were obtained:

1. The reinforcements are distributed uniformly in the laser cladding coating. The growth morphology of boundary is mainly in parallel branching dendrites.
2. The formation of parallel-branching has a range of the rate dendrite growth υ, which is correlated to the temperature gradient, liquidus temperature, the liquidus undercooling and the rate of pool solidification on the growing fronts.
3. A proper increasing convection E will be beneficial to distribution of elements in the cladding layer and the homogeneous microstructure of coating, and the convection mainly depended on the laser parameters, in this experimental conditions, a appropriate parameters are laser power of 2.0–2.5 kW, scanning speed of 4–8 mm/s and powder feed rate of 10–15 mg/s.
4. Compared with the AZ91D substrate, the wear resistance of the laser cladding coatings with Al + Al_2O_3 was improved.

Acknowledgements The work financially supported provided by the Inner Mongolia Educational Department of Science and Technology of China (No. NJ04006) and by Project 985-Automotive Engineering of Jilin University.

References

1. Han BQ, Dunand DC (2000) Mater Sci Eng A227:297
2. Jiang QC, Wang HY, Ma BX, Wang Y, Zhao F (2004) J Alloys Compd 386
3. Kim JM, Shin K, Kim KT, Jung WJ (2003) Scripta Mater 49:687
4. Wang HY, Jiang QC, Li XL, Wang JG (2003) Scripta Mater 48:1439
5. Rudd AL, Breslina CB, Mansfeld F (2000) Corros Sci 42:275
6. Gray JE, Luan B (2002) J Alloys Compd 336:88
7. Dutta Majumdar J, Galun R, Mordike BL, Manna I (2003) Mater Sci Eng A361:119
8. Galun R, Weisheit A, Mordike BL, Kainer KU (eds) (1998) Werkstoff informations-gesellschaft mbh, Germany, p 439
9. Maeng DY, Lee JH, Hong SI, ChunBS (2001) Mater Sci Eng A 311:128
10. Chen Y, Wang HM (2003) Mater Lett 57:1233
11. Wang HY, Jiang QC, Li XL, Zhao F (2004) J Alloys Compd 366:L9
12. De Hosson Th MJ, Kooi BJ (2001) Academic Press, New York, p 114
13. ASTM Standard (1986) Metals Park, vol 11, p 155
14. Kurz W, Fisher DJ (1998) Fundamentals of Solidification, 3rd rev edn. Trans Tech. Publications Ltd., p 137
15. Fisher DJ, Kurz W (1979) Coupled zone in faceted/non-faceted eutectics, In Solidification and Casting of Metal. The Metal Society, London, p 57
16. YT Pei, De Hosson JH, (2000) J Acta Mater 48:2617